

Stoichiometric change and solid decomposition in Ca-S compounds under high pressure

Yang Lv(吕阳), Jian-Fu Li(李建福), Zhao-Bin Zhang(张钊彬), Yong Liu(刘勇), Jia-Nan Yuan(袁嘉男), Jia-Ni Lin(林佳妮), and Xiao-Li Wang(王晓丽)

Citation : Chin. Phys. B, 2025, 34 (**4**): 046202. DOI: 10.1088/1674-1056/adb38e
Journal homepage: http://cpb.iphy.ac.cn; http://iopscience.iop.org/cpb

What follows is a list of articles you may be interested in

Pressure-driven crystal structure evolution in RbB_2C_4 compounds

Jinyu Liu(刘金禹), Ailing Liu(刘爱玲), Yujia Wang(王雨佳), Lili Gao(高丽丽), Xiangyi Luo(罗香怡), and Miao Zhang(张淼)

Chin. Phys. B, 2025, 34 (**4**): 046201. DOI: 10.1088/1674-1056/adb271

Novel high-temperature-resistant material $SbLaO_3$ with superior hardness under high pressure

Haoqi Chen(陈浩琦), Haowen Jiang(姜皓文), Xuehui Jiang(姜雪辉), Jialin Wang(王佳琳), Chengyao Zhang(张铖瑶), Defang Duan(段德芳), Jing Dong(董晶), and Yanbin Ma(马艳斌)

Chin. Phys. B, 2025, 34 (**2**): 026201. DOI: 10.1088/1674-1056/ad989e

Theoretical insights into the structures and fundamental properties of pnictogen nitrides

Jingjing Wang(王晶晶), Panlong Kong(孔攀龙), Dingmei Zhang(张定梅), Defang Gao(高德芳), Zaifu Jiang(蒋再富), and Wei Dai(戴伟)

Chin. Phys. B, 2024, 33 (**9**): 096201. DOI: 10.1088/1674-1056/ad6a07

High-pressure study on calcium azide ($Ca(N_3)_2$): Bending of azide ions stabilizes the structure

Xiaoxin Wu(武晓鑫), Yingjian Wang(王颖健), Siqi Li(李思琪), Juncheng Lv(吕俊呈), Jingshu Wang(王婧姝), Lihua Yang(杨丽华), Qi Zhang(张旗), Yanqing Liu(刘艳清), Junkai Zhang(张俊凯), and Hongsheng Jia(贾洪声)

Chin. Phys. B, 2024, 33 (**5**): 056201. DOI: 10.1088/1674-1056/ad2b53

Stability and melting behavior of boron phosphide under high pressure

Wenjia Liang(梁文嘉), Xiaojun Xiang(向晓君), Qian Li(李倩), Hao Liang(梁浩), and Fang Peng(彭放)

Chin. Phys. B, 2024, 33 (**4**): 046201. DOI: 10.1088/1674-1056/ad23d4

SPECIAL TOPIC — Structures and properties of materials under high pressure

Stoichiometric change and solid decomposition in Ca–S compounds under high pressure

Yang Lv(吕阳), Jian-Fu Li(李建福)[†], Zhao-Bin Zhang(张钊彬), Yong Liu(刘勇), Jia-Nan Yuan(袁嘉男), Jia-Ni Lin(林佳妮), and Xiao-Li Wang(王晓丽)[‡]

School of Physics and Electronic Information, Yantai University, Yantai 264005, *China*

(Received 16 December 2024; revised manuscript received 30 January 2025; accepted manuscript online 7 February 2025)

As an independent thermodynamic parameter, pressure significantly influences interatomic distances, leading to an increase in material density. In this work, we employ the CALYPSO structure search and density functional theory calculations to explore the structural phase transitions and electronic properties of calcium–sulfur compounds (Ca_xS_{1-x}, where $x = 1/4$, 1/3, 1/2, 2/3, 3/4, 4/5) under 0–1200 GPa. The calculated formation enthalpies suggest that Ca_xS_{1-x} compounds undergo multiple phase transitions and eventually decompose into elemental Ca and S, challenging the traditional view that pressure stabilizes and densifies compounds. The analysis of formation enthalpy indicates that an increase in pressure leads to a rise in internal energy and the *PV* term, resulting in thermodynamic instability. Bader charge analysis reveals that this phenomenon is attributed to a decrease in charge transfer under high pressure. The activation of Ca-3d orbitals is significantly enhanced under pressure, leading to competition with Ca-4s orbitals and S-3p orbitals. This may cause the formation enthalpy minimum on the convex hull to shift sequentially from CaS to CaS_3, then to Ca_3S and Ca_2S, and finally back to CaS. These findings provide critical insights into the behavior of alkaline-earth metal sulfides under high pressure, with implications for the synthesis and application of novel materials under extreme conditions and for understanding element distribution in planetary interiors.

Keywords: high pressure, calcium sulfide, stoichiometry, solid decomposition

PACS: 62.50.–p, 61.50.Ks, 82.40.Fp, 91.60.Gf

DOI: 10.1088/1674-1056/adb38e **CSTR:** 32038.14.CPB.adb38e

1. Introduction

Pressure is a critical thermodynamic parameter that compresses atomic distances and alters electronic structures, leading to electronic phase transitions, atomic rearrangements, and electron reconfiguration. This can give rise to unprecedented new phenomena, structures, properties, and theoretical frameworks.[1–6] Pressure has proven to be an essential tool for stabilizing unconventional stoichiometric compounds.[7] It has even enabled the formation of compounds between noble gases (NG) with closed-shell electronic structures and other elements. In recent years, the field of high-pressure physics has seen rapid development.[8] Experimentally, advancements in diamond anvil cell (DAC) technology have enabled hydrostatic pressures exceeding 900 GPa in laboratory settings and pressures in the TPa range under shock conditions.[9–13] These advancements drive exploration into new materials and properties under extreme pressure, pushing the boundaries of high-pressure research.

Under ambient pressure, alkaline earth metals exhibit a +2 oxidation state due to the significant energy gap between their active Ns^2 electrons and the outermost and second-lowest orbitals, which hinders orbital hybridization. Consequently, they are categorized as s-block elements. Under high pressure, however, alkaline earth metals exhibit complex orbital hybridization (e.g., s–p and s–d) and structural transitions, and some valence electrons may even localize in interstitial sites, forming interstitial quasiatoms (ISQs).[14,15] Under normal pressure, all alkaline earth chalcogenides, except MgTe and beryllium sulfide compounds, form fundamentally closed-shell ionic systems.[16] Alkaline earth chalcogenides (AECs) are abundantly present in the Earth's mantle at depths of 600 km to 2900 km, where pressures can reach up to 140 GPa. Compared to ambient conditions, these compounds' structures and electronic properties undergo significant changes under high pressure. The physical properties and band structures of AECs are quite similar; for example, they commonly exhibit a transition from the NaCl (B1) phase to the CsCl (B2) phase under pressure, except for BeS.[17–19] Their phase transitions and properties under relatively low pressures have been well studied and refined. Additionally, some of these compounds may become excellent superconductors under high temperatures.[20,21] AECs also have tremendous application potential, with high relevance to luminescent devices, microelectronic components, and catalysis in various industrial fields.[22–24]

[†]Corresponding author. E-mail: jianfuli@ytu.edu.cn

[‡]Corresponding author. E-mail: xlwang@ytu.edu.cn

© 2025 Chinese Physical Society and IOP Publishing Ltd. All rights, including for text and data mining, AI training, and similar technologies, are reserved.

CaS is a typical binary semiconductor among alkaline earth metal sulfides under ambient conditions in the CaS system. When doped with rare earth elements, CaS exhibits excellent luminescent properties, making it widely applicable.[24,25] In energy storage, CaS also shows significant potential; as early as 1974, it was reported as a promising solid electrolyte,[20] and in 1980, experiments confirmed its ionic conductivity, identifying it as a superionic conductor.[26] Subsequent studies have further elaborated on its conductive properties.[21] Recently, Ca_3S has been reported as a potential superconductor under high pressure. Additionally, in medical applications, CaS nanosheets have shown promise as an effective approach for cancer immunotherapy.[27]

Significant progress has been made in studying Ca–S compounds; however, much of this research has focused on their applications, with relatively limited investigation into their properties under high pressure. Furthermore, most existing studies have been conducted at pressures below 200 GPa, with few reports on novel high-pressure properties of these compounds. To our knowledge, high-pressure studies on Ca–S compounds with multiple stoichiometries remain scarce. This motivates us to explore this field further at higher pressures and deeper levels, aiming to uncover novel properties and phenomena under compression. The elements Ca and S belong to groups IIA and VIA, respectively, with Pauling electronegativity values of 1.00 and 2.58, suggesting that Ca–S compounds will predominantly exhibit ionic bonding. This high ionic character helps minimize the influences of covalent, metallic, or van der Waals interactions on compound stability, thereby allowing the effect of pressure-controlled ionic interactions on stability to be more direct and evident.

Using the CALYPSO (Crystal structural AnaLYsis by Particle Swarm Optimization) structure prediction method combined with first-principles calculations, we investigated the structural phase transitions and electronic behavior of calcium–sulfur compounds (Ca_xS_{1-x}, where $x = 1/4$, 1/3, 1/2, 2/3, 3/4, 4/5) under pressures ranging from 0 GPa to 1200 GPa. Several new high-pressure phases were predicted, and their thermodynamic and dynamic stabilities were characterized. Subsequently, we discovered a novel phenomenon in the Ca–S system: each compound in this system decomposes into its elemental constituents after undergoing several structural phase transitions. Interestingly, with increasing pressure, the composition with the lowest formation enthalpy shifts sequentially from CaS to CaS_3, then to Ca_3S and Ca_2S, and finally back to CaS. We comprehensively investigated these unique phenomena and provided new insights from various perspectives.

2. Computational details

The structure search software we employed is CALYPSO, which is based on a particle swarm optimization algorithm for crystal structure prediction.[28–30] This software has provided a highly effective means for research in various research areas.[31–37] The approach efficiently searches for stable structures based on a given chemical composition. We conducted searches using 1–4 formula units per primitive cell and investigated the stable phases of four compositions, namely, CaS_3, CaS_2, CaS, Ca_2S, Ca_3S, and Ca_4S. PSO-generated structures were used in a proportion of 60%, with a total of 20 generations and 50 structures per generation. CALYPSO performs structure search and subsequently calls VASP through an interface for initial structural optimization to obtain the energy of experimental structures and perform sorting. The lowest energy phase was selected for subsequent calculations. The software used in the next step is the Vienna *ab initio* simulation package (VASP) based on density functional theory (DFT) for first-principles calculations.[38,39] The Perdew, Burke, and Ernzerhof (PBE) generalized gradient approximation (GGA) was used for the electronic exchange–correlation function.[40,41] The electron–ion interactions were modeled utilizing the all-electron projector augmented wave (PAW) method.[42] A plane-wave cutoff energy of 700 eV and a k-point mesh with a minimum spacing of 0.2 Å were set for further geometry optimization and self-consistent calculations. The energy converged when the free energy and band structure energy variations between the two steps were less than 106 eV. To verify the stability of the newly discovered structures, the phonon dispersion was calculated using the phonopy code in density functional perturbation theory,[43] and Bader's quantum theory of atoms in molecules (QTAIM) analysis was performed.[44] The integrated crystal orbital overlap population (ICOHP) was calculated using the LOBSTER software package,[45,46] and the Madelung energy and chemical bonding were analyzed using VESTA.[47]

3. Results and discussion

3.1. Phase stability

Our results successfully reproduced the previously reported phase transition of CaS from the *Fm*-3*m* (B1) phase to the *Pm*-3*m* (B2) phase,[48] as well as the lowest enthalpy *P*-42$_1$*m* phase of CaS_3 at 50 GPa.[49] To determine the stable structures and phase transition sequence of the Ca–S system under pressure, we used the CALYPSO structure prediction method combined with first-principles calculations to perform structural searches for Ca_xS_{1-x} (where $x = 1/4$, 1/3, 1/2, 2/3, 3/4, 4/5) with 1–4 formula units in the 0–1200 GPa range. After obtaining the lowest-energy structures at specific pressures, we verified their thermodynamic stability using the Gibbs free energy (G) at 0 K, expressed as $G = U + PV + TS$. Since our theoretical calculations were conducted at $T = 0$ K, the Gibbs free energy reduces to the enthalpy (H), where $H = U + PV$.

The specific expression is

$$\Delta H(\mathrm{Ca}_x\mathrm{S}_y) = [H(\mathrm{Ca}_x\mathrm{S}_y) - xH(\mathrm{Ca}) - yH(\mathrm{S})]/(x+y).$$

For each stoichiometry, the structure with the lowest formation enthalpy at a given pressure is marked on the convex hull diagram, as shown in Fig. 1(a), to verify its thermodynamic stability. The lines in different colors represent various pressures, with solid dots indicating stable phases at each pressure. These stable phases do not tend to decompose into adjacent compounds or elemental constituents. In contrast, hollow dots represent compounds in a metastable state under the corresponding pressure.

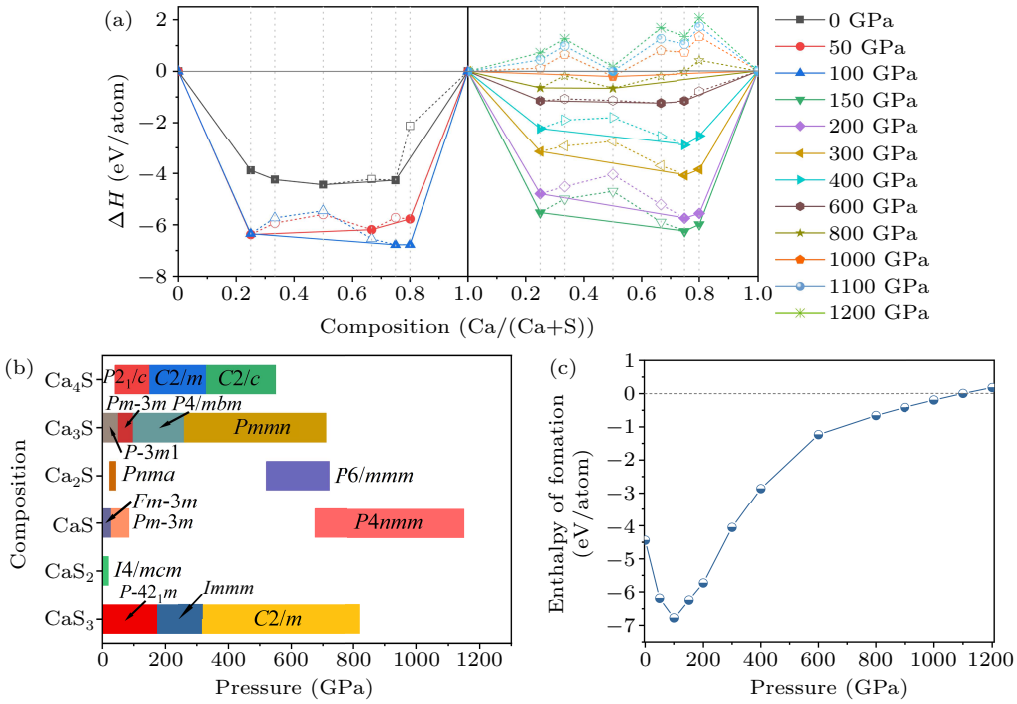


Fig. 1. Phase stability. Pressure–composition phase diagram and graph of the lowest formation enthalpy under different pressures of various Ca–S compounds. (a) Convex hull of Ca–S system. (b) Pressure phase diagram of Ca–S system. (c) The enthalpy of the compound with the lowest formation enthalpy in the system as a function of pressure.

3.2. The mechanism of pressure-induced decomposition

As shown in Fig. 1(a), within the 0–150 GPa range, the formation enthalpies of the compounds behave as expected, decreasing with increasing pressure and indicating enhanced stability. However, beyond 150 GPa, the positions of the formation enthalpies on the convex hull begin to turn upwards, indicating a decrease in thermodynamic stability. Consistent with previous studies, the structure with the lowest enthalpy at ambient pressure is CaS in the *Fm*-3*m* phase (with a lattice constant of 5.718 Å), as shown in Fig. 2(a). Upon increasing pressure, CaS transitions to the *Pm*-3*m* phase with a lattice constant of 3.070 Å, aligning well with prior research findings. At 50 GPa, the composition with the lowest enthalpy shifts towards sulfur-rich compounds, with CaS_3 in the space group of *P*-42$_1$*m* (Fig. 2(b)) having the lowest enthalpy, successfully reproducing previous experimental conclusions and validating the scientific rigor of our methodology. With further pressure increase, the stoichiometry with the lowest enthalpy shifts significantly towards calcium-rich compounds. At 100 GPa, the lowest-enthalpy compound in the Ca–S system is Ca_3S with the *P*4/*mbm* space group, as shown in Fig. 2(c). At 300 GPa, this compound transitions to the *Pmmn* space group, illustrated in Fig. 2(d). At 600 GPa, the composition with the lowest enthalpy shifts back toward sulfur-rich compounds, with Ca_2S in the *P*6/*mmm* space group (Fig. 2(e)) occupying the bottom of the convex hull. Meanwhile, the *P*4/*nmm* phase of CaS (Fig. 2(f)) approaches the convex hull line under increasing pressure, ultimately reaching the bottom of the hull at 800 GPa, becoming the lowest-enthalpy compound at that pressure. Finally, as pressure rises, the compound decomposes into elemental Ca and S at 1150 GPa.

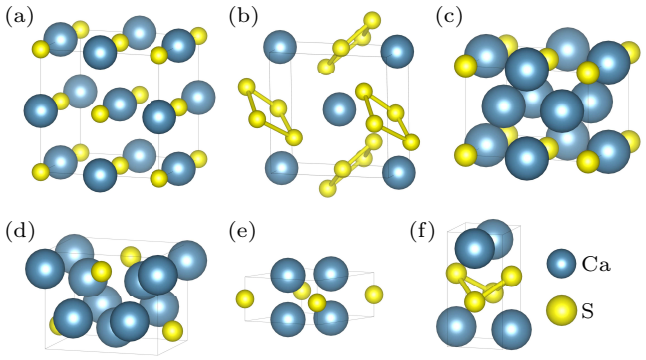


Fig. 2. Crystal structures and chemical bindings of the lowest enthalpy of formation in Ca–S compounds: (a) *Fm*-3*m* (CaS at 0 GPa), (b) *P*-42$_1$*m* (CaS_3 at 50 GPa), (c) *P*4/*mbm* (Ca_3S at 100 GPa), (d) *Pmmn* (Ca_3S at 300 GPa), (e) *P*6/*mmm* (Ca_2S at 600 GPa), (f) *P*4/*nmm* (CaS at 800 GPa).

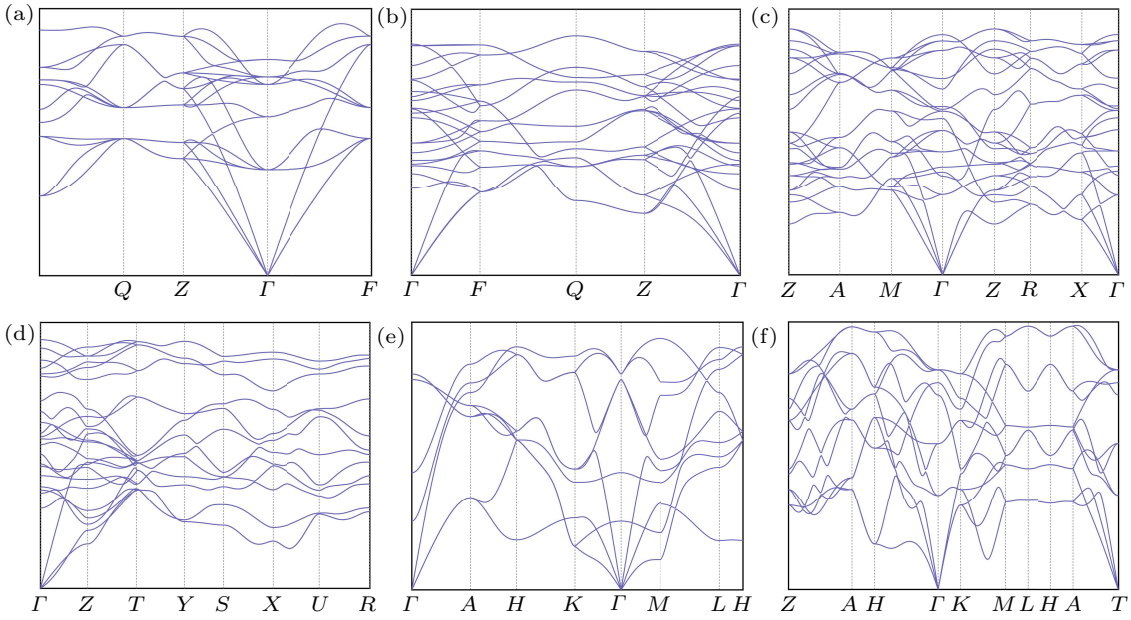


Fig. 3. Phonon spectrum of the lowest enthalpy compound in the Ca–S system: (a) *Fm*-3*m* (CaS at 0 GPa), (b) *P*-42$_1$*m* (CaS_3 at 50 GPa), (c) *P*4/*mbm* (Ca_3S at 100 GPa), (d) *Pmmn* (Ca_3S at 300 GPa), (e) *P*6/*mmm* (Ca_2S at 600 GPa), (f) *P*4/*nmm* (CaS at 800 GPa).

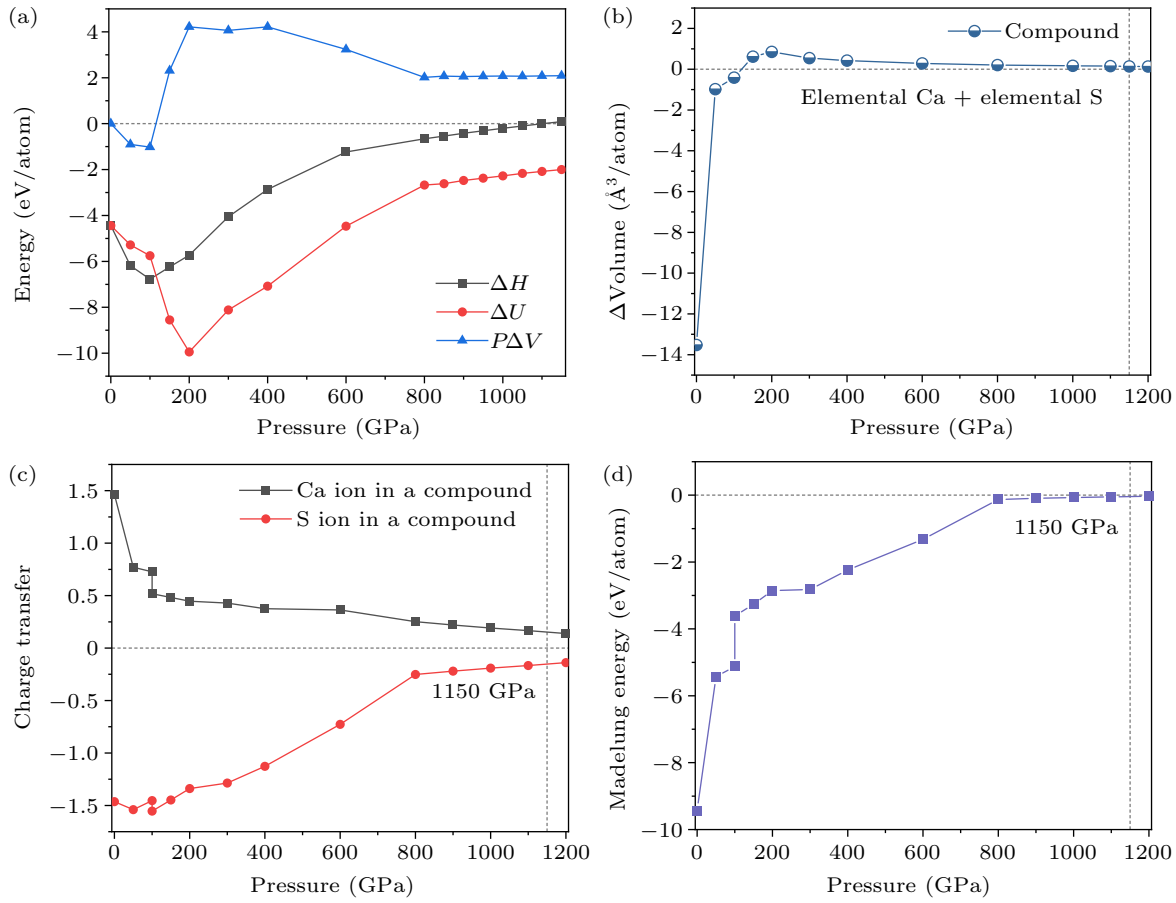


Fig. 4. High-pressure property analysis of Ca–S system. Each point in the figure is derived from the structure with the lowest formation enthalpy under that pressure: (a) ΔH, ΔU, and ΔPV versus pressure for Ca–S compounds. (b) The volume differences between the Ca–S compounds and elemental Ca and elemental S. (c) The Bader charge of Ca–S compounds. (d) The Madelung energy of Ca–S compounds.

We extracted these structures' formation enthalpies (H) and created an enthalpy difference diagram, as shown in Fig. 1(c). This diagram provides a clearer view of how the formation enthalpies decrease with increasing pressure, and then begin to rise after 150 GPa. When the pressure exceeds 1150 GPa, the formation enthalpy shifts from negative to positive, indicating that the compound decomposes into its elemental constituents. Across the entire pressure range, the

structures whose formation enthalpies are located at the bottom of the convex hull diagram are respectively observed as follows: *Fm*-3*m* (CaS) → *P*-42$_1$*m* (CaS$_3$) → *P*4/*mbm* (Ca$_3$S) → *Pmmn* (Ca$_3$S) → *P*6/*mmm* (Ca$_2$S) → *P*4/*nmm* (CaS). Apart from the first two phases, all other high-pressure phases are newly predicted in this study. Their crystal structure

Table 1. The parameters structures with the lowest formation enthalpy.

Space group	Pressure	Lattice parameter (Å)		Atom site		Wyckoff position		
CaS (Fm-3m)	0 GPa	$a=5.717$ $b=5.717$ $c=5.717$	$\alpha=90.00$ $\beta=90.00$ $\gamma=90.00$	Ca1	1a	0.500	0.500	0.500
				Ca2	1a	0.500	0.000	0.000
				Ca3	1a	0.000	0.500	0.000
				Ca4	1a	0.000	0.000	0.500
				S1	1a	0.500	0.500	0.000
				S2	1a	0.500	0.000	0.500
				S3	1a	0.000	0.500	0.500
				S4	1a	0.000	0.000	0.000
CaS$_3$ (P-42$_1m$)	50 GPa	$a=5.762$ $b=5.762$ $c=3.214$	$\alpha=90.00$ $\beta=90.00$ $\gamma=120.00$	Ca1	1a	0.000	0.000	0.500
				Ca2	1a	0.500	0.500	0.500
				S1	1a	0.699	0.199	0.003
				S3	1a	0.301	0.801	0.003
				S3	1a	0.199	0.301	0.997
				S4	1a	0.801	0.699	0.997
				S5	1a	0.000	0.500	0.616
				S6	1a	0.500	0.000	0.384
Ca$_3$S ($P$4/mbm)	100 GPa	$a=5.125$ $b=5.125$ $c=3.621$	$\alpha=90.00$ $\beta=90.00$ $\gamma=90.00$	Ca1	1a	0.500	0.000	0.000
				Ca2	1a	0.000	0.500	0.000
				Ca3	1a	0.750	0.250	0.500
				Ca4	1a	0.249	0.749	0.500
				Ca5	1a	0.250	0.250	0.500
				Ca6	1a	0.749	0.750	0.500
				S1	1a	0.000	0.000	0.000
				S2	1a	0.500	0.500	0.000
Ca$_3$S ($Pmmn$)	300 GPa	$a=3.657$ $b=4.688$ $c=3.893$	$\alpha=90.00$ $\beta=90.00$ $\gamma=90.00$	Ca1	1a	0.000	0.248	0.326
				Ca2	1a	0.500	0.252	0.674
				Ca3	1a	0.000	0.000	0.825
				Ca4	1a	0.500	0.500	0.175
				Ca5	1a	0.500	0.748	0.674
				Ca6	1a	0.000	0.751	0.326
				S1	1a	0.500	0.000	0.170
				S2	1a	0.000	0.500	0.830
Ca$_2$S ($P$6/mmm)	600 GPa	$a=3.388$ $b=3.388$ $c=1.985$	$\alpha=90.00$ $\beta=90.00$ $\gamma=120.00$	Ca1	1a	0.333	0.667	0.000
				Ca2	1a	0.667	0.333	0.000
				S	1a	0.000	0.000	0.500
CaS (P4/nmm)	800 GPa	$a=2.263$ $b=2.263$ $c=4.490$	$\alpha=90.00$ $\beta=90.00$ $\gamma=90.00$	Ca1	1a	0.000	0.500	0.868
				Ca2	1a	0.500	0.000	0.132
				S1	1a	0.000	0.500	0.400
				S2	1a	0.500	0.000	0.600

information is shown in Table 1. Furthermore, phonon calculations confirmed the dynamic stability of these phases at their respective transition pressures. As shown in Fig. 3, these structures have no imaginary frequencies at their corresponding pressures, affirming their dynamic stability under the relevant conditions. In addition, the phase transition sequences of various compositions in the Ca–S system are shown in Fig. 1(b), and the specific crystal information is presented in Table S1. Subsequently, we analyzed the band structures of the thermodynamically stable structures within the Ca–S system, thereby obtaining their band gaps, as presented in Table S2. It can be observed from the table that when the proportion of Ca ions in the compound (composition) exceeds 0.5, all the compounds manifest metallic properties. Analyzing the compounds with a Ca ion proportion less than or equal to 0.5 from the perspective of pressure, it can be discovered that the phases of the compounds at lower pressures all belong to semiconductors/insulators, but the band gaps of the high-pressure phases above 200 GPa are all closed, demonstrating metallic properties. This indicates that both the component ratio of the compound and the pressure can exert an influence on the band gap of the compounds.

In summary, the Ca–S compounds illustrated in Fig. 1(a) exhibit two unusual phenomena under increasing pressure. The first is an unexpected, pressure-induced reduction in thermodynamic stability, ultimately leading to decomposition into elemental constituents. The second phenomenon is a shift in the lowest formation enthalpy stoichiometry during the decomposition process.

To investigate the mechanism of pressure-induced decomposition, we analyzed the formation enthalpy of the lowest-enthalpy phase at each pressure and the enthalpy difference (ΔH) between it and the elemental mixture, using the formula $\Delta H = \Delta U + \Delta(PV)$. This enthalpy was separated into its internal energy (ΔU) and $\Delta(PV)$ components, as shown in Fig. 4(a). The results indicate that below 150 GPa, the reduction in formation enthalpy is due to a concurrent decrease in both internal energy (ΔU) and the $\Delta(PV)$ term. Above 150 GPa, the $\Delta(PV)$ term rises sharply, causing a gradual increase in ΔH. This is followed by a rise in internal energy after 200 GPa, leading to a rapid increase in ΔH. Beyond 800 GPa, the simultaneous rise in the $\Delta(PV)$ term and internal energy drives ΔH above zero, ultimately resulting in decomposition. The change in the $\Delta(PV)$ term can be explained by the volume difference between the compound (averaged per atom) and the elemental mixture as a function of pressure, as illustrated in Fig. 4(b). The plot shows that below 100 GPa, the compound has a significantly smaller volume than the mixture of elemental Ca and S, indicating that the compound is more compact and denser under these pressures. Consequently, elements are more likely to form compounds, resulting in a decrease in the Δ term and a reduction in ΔH in the 0–100 GPa range. However, above 150 GPa, the compound volume becomes notably larger than the elemental mixture's, suggesting that the mixture becomes more compact than the compound at these pressures. As a result, elements favor forming elemental phases over compounds, causing a rapid increase in the $\Delta(PV)$ term to positive values beyond 150 GPa, driving ΔH to increase.

Regarding the internal energy (ΔU), atomic interactions are critical. Given the substantial electronegativity difference in the Ca–S compound (1.58), ionic interactions are crucial in maintaining compound stability. We therefore used Bader charge analysis to investigate charge transfer at each pressure point. As shown in Fig. 4(c), the compound's charge transfer between Ca and S ions decreases consistently with increasing pressure. At the decomposition pressure (1150 GPa), the charge transfer between Ca and S ions has dropped to 0.1659, representing an 88.66% reduction over the 0–1150 GPa pressure range, indicating that ionic interactions within the compound have become minimal at 1150 GPa. To further verify this, we calculated the Madelung energy at each pressure point to quantify ionic interactions within the compound. Figure 4(d) shows that the Madelung energy trend closely aligns with the Bader charges. As anticipated, in the last stable phase before decomposition (800 GPa), the Madelung energy decreases to 0.129 eV and then to 0.0426 eV at 1150 GPa, matching well with the decomposition pressure.

Furthermore, we analyzed the occupation number and projected density of states (PDOS) of the compound to further explore the factors contributing to the observed reduction in charge transfer. As shown in Fig. 1(c), the formation enthalpy of the compound decreases from -4.441 eV to -6.776 eV within the pressure range of 0–100 GPa. This trend aligns with the general understanding that increasing pressure enhances the density and stability of materials. Meanwhile, in this pressure range, as illustrated in Fig. 5(b), a noticeable downshift is observed in the Ca-d orbitals, indicating their activation. Simultaneously, the S-p orbitals also exhibit a downshift, suggesting activation under pressure. We infer that, although the Ca-d orbitals are activated and become more occupied, as shown in Fig. 5(a), the S-p orbitals also experience increased occupation and activation under pressure. Consequently, the Ca-d orbitals do not yet exhibit a clear dominance over the S-p orbitals, resulting in an overall stabilization of the compound. Subsequently, in the pressure range of 100–1150 GPa, the formation enthalpy, as depicted in Fig. 1(c), dramatically decreases from -6.776 eV to 0 eV. This substantial reduction is primarily attributed to the weakening of charge transfer described earlier. The weakening of charge transfer can be further elucidated by examining the changes in PDOS shown in Fig. 5(b). Within the pressure range of 100–800 GPa, a pronounced downshift in the Ca-d orbitals

is evident, reflecting significant activation and increased electron occupation of these orbitals under pressure. Concurrently, the electron occupation of the S-p orbitals decreases. This redistribution of electronic states ultimately reduces the charge transfer between elements within the compound, leading to the decomposition of the system into its elemental constituents.

In conclusion, the decomposition of Ca–S compounds under high pressure is primarily driven by two factors. The main factor is the significant reduction in charge transfer with increasing pressure, which weakens ionic bonds and increases the ΔU term. Additionally, under high pressure, the elemental mixture becomes more volume-efficient than the compound, causing the $\Delta(PV)$ term to remain positive above 170 GPa. Ultimately, the combined effect of these two factors raises the ΔH value above zero, resulting in the decomposition of the compound.

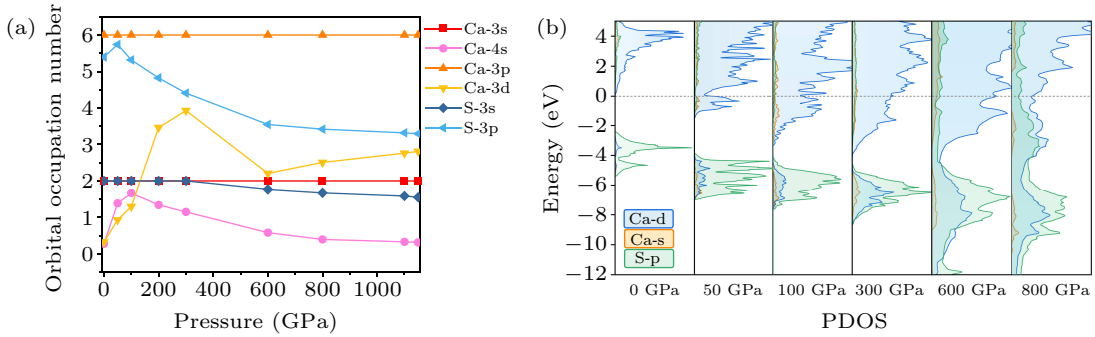


Fig. 5. (a) Orbital occupation number of Ca–S compounds as a function of pressure. Each point in the figure is derived from the structure with the lowest formation enthalpy under that pressure. (b) PDOS diagram of Ca–S compounds under different pressures. In the figure, the PDOS at each pressure is derived from the structure with the lowest formation enthalpy under that pressure.

3.3. The mechanism of the shift in stoichiometry

To further investigate the observed shifting of the lowest formation enthalpy Ca–S compound from CaS to CaS_3, then to Ca_3S and Ca_2S, before eventually returning to CaS, we calculated the orbital occupation numbers and electron projected density of states (PDOS) of the compounds to gain deeper insight into this phenomenon from an electronic property perspective. As shown in Fig. 5(a), it is evident that the occupation of the Ca 3d and 4s orbitals increases significantly below 100 GPa, indicating that in the pressure range of 0–100 GPa, despite an overall energy increase across all orbitals, the increased occupation of the Ca-3d, Ca-4s, and S-3p orbitals can indirectly reflect that their orbital energies are lower than those of other orbitals and are in a state of enhanced activation. At the same time, the steep slopes of these two orbitals for Ca at pressures from 0 GPa to 50 GPa demonstrate that their electron occupancy grows faster than that of the S-3p orbital under equivalent pressure conditions. It can also be observed from Fig. 5(b) that, in contrast to the DOS plot at 0 GPa, the occupation of the Ca-3d and Ca-4s orbitals below the Fermi surface increases significantly at 50 GPa. Consequently, Ca ions exhibit an enhanced reductive character in this range, causing the composition with lowest formation enthalpy in the Ca–S system to shift from CaS to CaS_3 around 50 GPa. Between 50 GPa and 100 GPa, the occupation of both the Ca-3d and Ca-4s orbitals continues to increase, with Ca-4s occupation rising from 0.27 (0 GPa) to 1.67 (100 GPa), and Ca-3d occupation increasing from 0.32 (0 GPa) to 1.30 (100 GPa). Combining with Fig. 5(b), the Ca-4s and Ca-3d orbitals shift downward at 100 GPa compared to 50 GPa, indicating that both the Ca-4s and Ca-3d orbital activation are increasing. This shows an apparent competitive attraction for electrons within Ca, which may increase internal electron transfer and reduce Ca's reductive character. Consequently, in this pressure range, more Ca ions are required to reduce S ions, shifting the composition with lowest formation enthalpy in the Ca–S system from CaS_3 to Ca_3S. From 100 GPa to 600 GPa, the occupation of the Ca-3d orbital surpasses that of the Ca-4s orbital, attracting electrons from Ca-4s to the Ca-3d orbital. As pressure increases, from 600 GPa to 1150 GPa, Ca's 4s electrons are nearly depleted. This may diminish internal electron transfer and extend the Ca-3d orbital's energetic influence beyond atomic boundaries to interionic interactions within the compounds. It can also be discerned from Fig. 5(b) that the Ca-3d orbital has been shifting downward with the increase in pressure, suggesting a highly conspicuous activation of the Ca-3d orbital under pressure. This results in a resurgence of Ca's reductive behavior, the compound with lowest formation enthalpy shifting from CaS to CaS_3, then to Ca_3S and Ca_2S, and finally returning to CaS.

Additionally, in the pressure range of 0–50 GPa, the occupation of the S-3p orbital is observed to increase, suggesting that the interaction between Ca and S ions intensifies, thereby enhancing the stability of the compound. Beyond this range, from 50 GPa to 1150 GPa, the S-3p orbital occupation gradually decreases, indicating a weakening of the ionic interaction between atoms under increasing pressure. This further supports the previously proposed mechanism behind the decomposition of the compound. As pressure rises, the gradual reduction in S-3p electron occupation aligns with the diminished ionic interactions discussed earlier. This decreasing

trend underscores the progressive reduction of charge transfer and ionic bonding strength in the compound, which eventually contributes to the compound's decomposition at very high pressures. Thus, this trend in orbital occupation reinforces the physical mechanism of pressure-induced decomposition as previously described.

4. Conclusion

We have used the CALYPSO structure prediction method combined with first-principles calculations to study the structural phase transitions and electronic behavior of calcium sulfide compounds (Ca_xS_{1-x}, $x = 1/4$, 1/3, 1/2, 2/3, 3/4, 4/5) in the pressure range of 0–1200 GPa, and predicted several new high-pressure phases. Under sufficient compression (0–1150 GPa), our work provides new insights into two new phenomena of pressure-induced decomposition and the shift in the stoichiometry of the lowest enthalpy compound. For the pressure-induced decomposition phenomenon, we further analyzed the ΔH. We found that the primary cause of the decomposition is the decrease in charge transfer between Ca and S ions, from 1.465 *e*/atom to 0.139 *e*/atom, within the compound as pressure increases. This reduction weakens the ionic bonds, leading to a sharp rise in the ΔU of the compound. The significant rise in Madelung energy (from −9.434 eV/atom to −0.035 eV/atom) further confirms this weakening of ionic interactions, which ultimately contributes to the decomposition of the compound at high pressures. Additionally, the denser volume of the Ca and S elemental mixture relative to the Ca–S compound after 170 GPa leads to a rapid increase in the ΔV, which then turns positive. This provides the second key reason for the pressure-induced decomposition of the compound. The shift in the stoichiometry of the compound might be due to the activation of Ca-3d orbitals under pressure, which may account for this phenomenon, leading to their competition with Ca-4s and S-3p orbitals. This competition can cause a change in the oxidation-reduction behavior of the Ca element, which initially weakens, then enhances, and finally weakens again. This explains the observed phenomenon of the lowest enthalpy compound shifting from CaS to CaS_3, then to Ca_3S and Ca_2S, and finally returning to CaS under pressure. These results offer new insights and understanding in studying alkaline earth chalcogenide compounds under extreme conditions and have important implications for geological research, as well as material synthesis and applications.

Acknowledgments

Project supported by the National Natural Science Foundation of China (Grant Nos. 11974154 and 12304278), the Taishan Scholars Special Funding for Construction Projects (Grant No. tstp20230622), the Natural Science Foundation of Shandong Province (Grant Nos. ZR2022MA004, ZR2023QA127, and ZR2024QA121), and the Special Foundation of Yantai for Leading Talents above Provincial Level.

References

[1] Miao M, Sun Y, Zurek E and Lin H 2020 *Nat. Rev. Chem.* **4** 508
[2] Zhai H, Xu R, Dai J, Ma X, Yu X, Li Q and Ma Y 2022 *J. Am. Chem. Soc.* **144** 21640
[3] Li J, Geng Y, Xu Z, Zhang P, Garbarino G, Miao M, Hu Q and Wang X 2022 *JACS Au* 3 402
[4] Hu P, Peng J, Xie X, Wen M, Zhang X, Wu F and Dong H 2022 *Chin. Phys. B* **31** 036301
[5] Xie H, Wang J, Wang L, Yan Y, Guo J, Gao Q, Chao M, Liang E and Ren X 2022 *Chin. Phys. B* **31** 076101
[6] Chen B, Tian M, Zhang J, Li B, Xiao Y, Chow P, Kenney-Benson C, Deng H, Zhang J,Ding Y and Mao H K, *et al.* 2022 *Phys. Rev. Lett.* **129** 016401
[7] Li B, Liu H, Zhong X and Liu G 2022 *Phys. Rev. Res.* **4** 033082
[8] Zhu L, Liu H, Pickard C J, Zou G and Ma Y 2014 *Nat. Chem.* **6** 644
[9] Dubrovinsky L, Khandarkhaeva S, Fedotenko T, Laniel, Bykov M, Giacobbe, Lawrence Bright E, Sedmak, Chariton, Prakapenka, Ponomareva A, Smirnova E, Belov M P, Tasádi F, Shulumba, Trybel, Abrikosov I A and Dubrovinskaia N 2022 *Nature* **605** 274
[10] Mikhailova O L, Mochalov M A, Sokolova A I and Urlin V D 2000 *High Temperature* **38** 210
[11] Ragan III C E 1980 *Phys. Rev. A* **21** 458
[12] Anzellini S and Boccato S 2020 *Crystals* **10** 459
[13] Liu J, Tao Y, Fan C, Wu B, Tang Q and Lei L 2022 *Chin. Phys. B* **31** 037801
[14] Li F, Zhang X, Fu Y, Wang Y, Bergara A and Yang G 2021 *J. Phys. Chem. Lett.* **12** 4203
[15] Rahm M, Cammi R, Ashcroft N W and Hoffmann R 2019 *J. Am. Chem. Soc.* **141** 10253
[16] Khenata R, Sahnoun M, Baltache, Rérat, Rached, Driz M and Bouhafs B 2006 *Physica B* **371** 1
[17] Potzel O and Taubmann G 2011 *J. Solid State Chem.* **184** 1079
[18] Varshney D, Kaurav N, Sharma U and Singh R K 2008 *J. Phys. Chem. Solids* **69** 60
[19] Boucenna S, Medkour Y, Louail L, Boucenna M, Hachemi A and Roumili A 2013 *Comput. Mater. Sci.* **68** 325
[20] Nagata K and Goto K S 1974 *Metallurgical Transactions* **5** 899
[21] Egami A, Onoye T and Narita K 1981 *Transactions of the Japan Institute of Metals* **22** 399
[22] Ali R, Mohammad S, Ullah H, Khan S A, Uddin H, Khan M and Khan N U 2013 *Physica B* **410** 93
[23] Rao R P 1986 *J. Mater. Sci.* **21** 3357
[24] Naeemullah, Murtaza G, Khenata R, Safeer A, Alahmed Z A and Bin Omran S 2014 *Comput. Mater. Sci.* **91** 43
[25] Yasuhiro Nakao 1980 *J. Phys. Soc. Japan* **48** 534
[26] Hiroaki Nakamura and Gunji Koki 1980 *Transactions of the Japan Institute of Metals* **21** 375
[27] Yu Q, Li Q, Tu L, Zhou Y, Zhu H, Zhang Q, Liu M and Sun Y 2023 *Chem. Eng. J.* **477** 147085
[28] Wang Y, Lv J, Zhu L and Ma Y 2010 *Phys. Rev. B* **82** 094116
[29] Wang Y, Lv J, Zhu L and Ma Y 2012 *Comput. Phys. Commun.* **183** 2063
[30] Gao B, Gao P, Lu S, Lv J, Wang Y and Ma Y 2019 *Sci. Bull.* **64** 301
[31] Lv Y, Li J, Zhang Z, Geng Y, Xu Z, Liu Y, Yuan J, Wang Q and Wang X 2024 *Phys. Chem. Chem. Phys.* **26** 10399
[32] Xu Z, Li J, Geng Y, Zhang Z, Lv Y, Zhang C, Wang Q and Wang X 2023 *Chin. Phys. Lett.* **40** 076201
[33] Geng Y, Li J, Zhang Z, Lv Y, Lu M, Zhu M, Liu Y, Yuan J, Hu Q and Wang X 2024 *Matter and Radiation at Extremes* **9** 067804
[34] Geng Y, Li J, Zhang Z, Lv Y, Xu Z, Liu Y, Yuan J, Wang Q and Wang X 2023 *Phys. Chem. Chem. Phys.* **25** 23448
[35] Liu Y, Li J, Geng Y, Xu Z, Lv Y, Zhang Z, Yuan J and Wang X 2024 *Physica B* **681** 415846
[36] Zhang Z, Li J, Lv Y, Geng Y, Xu Z, Liu Y, Yuan J and Wang X 2024 *Comput. Mater Sci.* **231** 112593
[37] Xu Z, Rui Q, Geng Y, Li J, Wang Q and Wang X 2022 *Europhys. Lett.* **140** 16003
[38] Wang Y and Perdew J P 1991 *Phys. Rev. B* **43** 891

[39] Kresse G and Furthmü J 1996 *Phys. Rev. B* **54** 11169
[40] Perdew J P, Burke K and Ernzerhof M 1996 *Phys. Rev. Lett.* **77** 386
[41] Perdew J P and Wang Y 1992 *Phys. Rev. B* **45** 13244
[42] Blochl P E 1994 *Phys. Rev. B* **50** 17953
[43] Ozturk K, Zhong Y U, Chen L Q, Wolverton C, Sofo J O and Liu Z K 2005 *Metallurgical and Materials Transactions A* **36** 5
[44] Tang W, Sanville E and Henkelman G 2009 *J. Phys. Condens. Matter* **21** 084204
[45] Deringer V, Tchougréeff A L and Dronskowski R 2011 *J. Phys. Chem. A* **115** 5461
[46] Maintz S, Deringer V L, Tchougréeff A L and Dronskowski R 2016 *J. Comput. Chem.* **37** 1030
[47] Momma K and Izumi F 2011 *J. Appl. Crystallogr.* **44** 1272
[48] Feng H, Wang S and Wu B 2022 *J. Phys. Conf. Ser.* **2148** 012015
[49] Wang S, Lu W, Liu S, Zhou M, Gao P, Wang H, Lv J, Gou H, Liu G, Liu H, Wang Y and Ma Y 2021 *Phys. Rev. B* **104** 054117